

Coexistence of Magnetic and Electric Orderings in the Metal–Formate Frameworks of $[\text{NH}_4][\text{M}(\text{HCOO})_3]$

Guan-Cheng Xu,[†] Wen Zhang,[‡] Xiao-Ming Ma,[†] Yi-Hong Chen,[†] Li Zhang,[†] Hong-Ling Cai,[‡] Zhe-Ming Wang,^{*,†} Ren-Gen Xiong,^{*,†} and Song Gao^{*,†}

[†]Beijing National Laboratory for Molecular Sciences, State Key Laboratory of Rare Earth Materials Chemistry and Applications, College of Chemistry and Molecular Engineering, Peking University, Beijing 100871, P.R. China

[‡]Ordered Matter Science Research Center, Southeast University, Nanjing 211189, P.R. China

S Supporting Information

ABSTRACT: A family of three-dimensional chiral metal–formate frameworks of $[\text{NH}_4][\text{M}(\text{HCOO})_3]$ ($\text{M} = \text{Mn}, \text{Fe}, \text{Co}, \text{Ni}, \text{and Zn}$) displays paraelectric to ferroelectric phase transitions between 191 and 254 K, triggered by disorder–order transitions of NH_4^+ cations and their displacement within the framework channels, combined with spin-canted antiferromagnetic ordering within 8–30 K for the magnetic members, providing a new class of metal–organic frameworks showing the coexistence of magnetic and electric orderings.

In their article, “There is plenty of room in the middle”, Cheetham and Rao¹ claimed many opportunities and potentials for use of metal–organic frameworks (MOFs, the “middle”) beyond purely organic or inorganic systems because of their organic–inorganic hybrid character. Indeed, this continues to be realized by rapidly developing research on MOFs.^{1,2} Having shown a very wide spectrum of functionalities, properties, and possible applications, MOFs are promising for magnetism and ferro/antiferroelectrics because, within MOFs, (i) magnetic metal ions and their coupling can be introduced and tailored³ and (ii) H-bonding systems and/or polar components required for ferro/antiferroelectrics in molecule-based materials,⁴ such as those in traditional KDP and TGS,⁵ and recently organic ones,⁶ are easily achieved and controlled if suitable components or building blocks are chosen and properly organized in these hybrid materials. Furthermore, if these two aspects are combined, multiferroic MOFs can be created,⁷ though examples are still very rare. Multiferroics have attracted considerable attention in recent years due to their fundamental scientific interest and their potential applications in new devices based on the mutual control of magnetic and electric fields.⁸ However, molecule-based multiferroic materials are still in want of exploration. In this context, we and some others have started to explore metal–formate frameworks.^{9–15} These MOFs seem to be suitable candidates for multiferroics because both requirements mentioned above can be satisfied in such systems. Kobayashi et al. found interesting dielectric properties—even ferroelectricity—in the porous magnetic framework of $[\text{Mn}_3(\text{HCOO})_6]$ with water, methanol, and ethanol as polar guests.¹⁰ Cheetham et al.¹¹ reported a class of multiferroic MOFs, $[(\text{CH}_3)_2\text{NH}_2][\text{M}(\text{HCOO})_3]$ ($\text{M} = \text{Mn}, \text{Fe}, \text{Co}, \text{Ni}, \text{and Zn}$), in which the magnetic members show magnetic ordering at 8–36 K, as first reported by us,¹² and antiferroelectric

ordering at 160–185 K. A possible magnetoelectric effect has recently been suggested for the metal–formate pervoskite $[\text{C}(\text{NH}_2)_3][\text{Cu}(\text{HCOO})_3]$.¹³ Very recently, we have observed that the chiral metal–formate framework $[\text{NH}_4][\text{Zn}(\text{HCOO})_3]$ shows ferroelectric property below 191 K, originating from the ordering of the hydrogen-bonding system.¹⁴ It is noteworthy that the magnetic analogues¹⁵ of $[\text{NH}_4][\text{M}(\text{HCOO})_3]$ are possible multiferroics. In this Communication, we report the study of this family for $\text{M} = \text{Mn}$ (**1Mn**), Fe (**2Fe**), Co (**3Co**), Ni (**4Ni**), and $[\text{NH}_4][\text{Zn}(\text{HCOO})_3]$ (**5Zn**). They show weak ferromagnetism (for the magnetic members, Mn to Ni) and ferroelectricity at low temperatures, characterized by single-crystal X-ray diffraction, magnetic investigation, dielectric anomaly, electric hysteresis loop, and differential scanning calorimetry (DSC). Ammonium compounds such as ammonium sulfate, ammonium fluoberyllate, and some ammonium alums are long-known ferroelectrics,⁵ and new ones^{8d,16} have lately attracted attention again.

The compounds of the $[\text{NH}_4][\text{M}(\text{HCOO})_3]$ series can be prepared by reaction of ammonium formate, formic acid, and suitable divalent metal salts in methanol (see the Supporting Information (SI)) as described previously.^{14,15} Except for **4Ni**, slow diffusion methods afforded big hexagonal plate or bipyramidal crystals (Figure S1) for dielectric measurements. The bulk phase purity was confirmed by powder X-ray diffraction (Figure S2).

The magnetic properties of **1Mn**, **3Co**, and **4Ni** were re-investigated (see SI), and the occurrence of weak ferromagnetism within the three materials was confirmed (Figure 1). Long-range ordering of spin-canted antiferromagnetism occurred at 8.0, 9.8, and 29.3 K for **1Mn**, **3Co**, and **4Ni**, respectively, in line with the previous study.^{15a} The investigation^{15b} on **2Fe** revealed that it is a weak ferromagnet with $T_C = 9.4$ K. Hidden spin-canting is likely for these materials because of their observed small, spontaneous magnetization values compared to other metal–formate series^{9,13b} and the tripling of lattice due to the paraelectric–ferroelectric phase transition (see below), which results in multiple sublattices for hidden spin-canting.^{17,12a}

The five materials were subjected preliminary DSC measurements (Figure 2, under heating). Endothermic peaks on DSC traces were observed at 254 (**1Mn**), 212 (**2Fe**), 191 (**3Co**), 199 (**4Ni**), and 192 K (**5Zn**), corresponding to the phase transition,

Received: July 23, 2011

Published: August 26, 2011

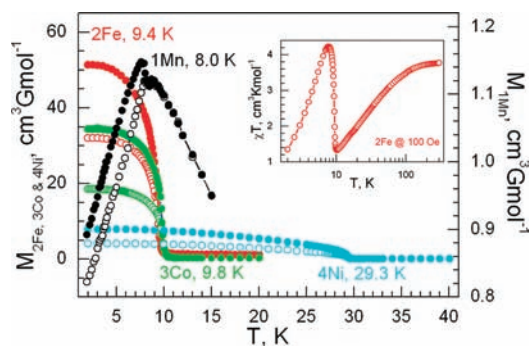


Figure 1. Zero-field-cooled (open symbols) and field-cooled (filled symbols) magnetization plots of the **1Mn**, **2Fe**, **3Co**, and **4Ni** under 5 or 10 Oe fields. Inset: temperature dependence of the magnetic susceptibility of **2Fe** under 100 Oe field.

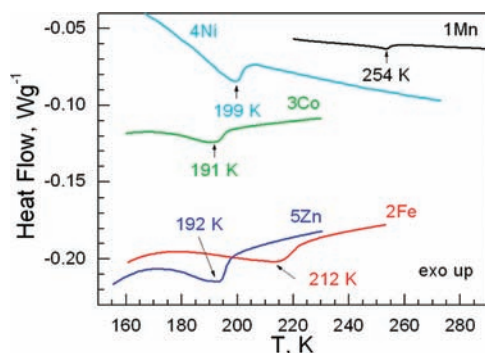


Figure 2. Low-temperature DSC traces for **1Mn**, **2Fe**, **3Co**, **4Ni**, and **5Zn** in heating mode.

and these define the phase transition temperatures. The ΔH values were estimated to be ~ 0.2 – 0.4 kJ mol $^{-1}$. **1Mn** and **2Fe** seem to have broader peaks than **3Co**, **4Ni**, and **5Zn**, and these different thermal dispersion behaviors might be related to their dielectric properties.

Except for **4Ni**, for which a large crystal is still unavailable, dielectric permittivity and polarization properties have been investigated on single crystals of **1Mn**, **2Fe**, **3Co**, and **5Zn**¹⁴ along the *c* and *a* axes (Figure 3 and Figures S3–S5). Temperature-dependent traces of the real components ϵ' of dielectric permittivities under an applied electric field $E//c$ with a frequency of 10 kHz (Figure 3) for the four materials show high dielectric anomaly peaks, and at the peak positions the ϵ' values are several to tens times larger than those in higher or lower temperature regions. In more detail, the peak temperatures/ ϵ' values at 10 kHz are 246 K/78 (**1Mn**), 170 K/330 (**2Fe**), 193 K/879 (**3Co**), and 191 K/606 (**5Zn**), while at room temperature/around 20 K the ϵ' values are 46/8.6 (**1Mn**), 92/10 (**2Fe**), 81/5.7 (**3Co**), and 63/17 (**5Zn**), respectively. For **3Co** and **5Zn** the peak temperatures are close to those observed in DSC, while for **1Mn** and **2Fe** the difference is significant, i.e., 246 vs 254 K and 170 vs 212 K for **1Mn** and **2Fe**, respectively. The ϵ' data of **3Co** at 10 kHz above 230 K fit the Curie–Weiss law well (Figure S3), and the fitting afforded a Curie constant of 8.26×10^3 K, comparable to those of ferroelectrics undergoing disorder–order transitions of H-bonding systems, such as KDP, TGS, and RS,^{5,6b} and a Weiss temperature of 187 K, slightly

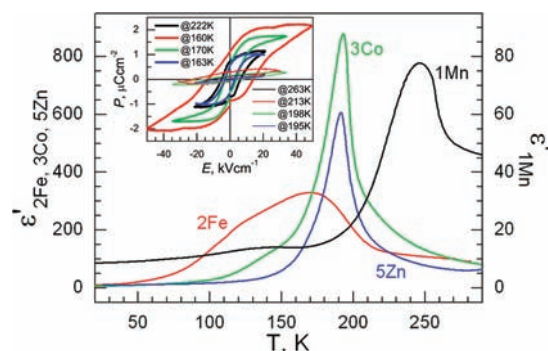


Figure 3. Temperature-dependent traces of the real part of the dielectric permittivities, ϵ' , for **1Mn**, **2Fe**, **3Co**, and **5Zn**, with $E//c$ at 10 kHz. Inset: electric hysteresis loops for the four materials at temperatures below and above the transition points, with $E//c$.

lower than the peak temperature of 191 K. For **5Zn**, the Curie constant is 5.39×10^3 K and the Weiss temperature is 181 K (Figure S3).¹⁴ Both **3Co** and **5Zn** show quite sharp and narrow peaks. In contrast, **1Mn** and **2Fe** display wide peaks—especially **2Fe** has a quite expanded peak spanning from 50 to 220 K with a shoulder around 120 K—and the high-temperature ϵ' data deviate from the Curie–Weiss law (Figure S3). **1Mn** shows an additional small, flat peak around 135 K. In fact, **3Co** also has a shoulder around 140 K, although it is not very significant at 10 kHz. The ϵ' vs *T* traces at 1, 10, 100, and 1000 kHz are shown in Figure S4. The main peak positions display slight frequency dependence, while the shoulders of **2Fe** and **3Co** and the small, flat peak of **1Mn** become more significant and move to lower temperatures at increased frequencies. These results indicate the relaxor-like characteristics^{18,19} of the materials. Relaxor ferroelectricity has been documented in some H-bonding systems.¹⁹

While the above dielectric studies revealed that **1Mn**, **2Fe**, and **3Co** are ferroelectrics, like **5Zn**,¹⁴ the electric hysteresis loops (Figure 3, inset), with the applied electric field $E//c$ axis, clearly occurred below the phase transition temperatures, and spontaneous polarizations increased with decreasing temperatures (data not given here). At the lowest temperatures used, the observed saturation spontaneous polarizations (P_S), the remnant polarizations (P_R), and the coercive fields (E_C) were $0.97 \mu\text{C cm}^{-2}$, $0.72 \mu\text{C cm}^{-2}$, and 5.1 kV cm^{-1} for **1Mn**; $2.2 \mu\text{C cm}^{-2}$, $1.1 \mu\text{C cm}^{-2}$, and 13.5 kV cm^{-1} for **2Fe**; $1.6 \mu\text{C cm}^{-2}$, $0.6 \mu\text{C cm}^{-2}$, and 3.0 kV cm^{-1} for **3Co**; and $1.03 \mu\text{C cm}^{-2}$, $0.68 \mu\text{C cm}^{-2}$, and 2.8 kV cm^{-1} for **5Zn**. The observation of larger P_S values for **2Fe** and **3Co** than expected (0.94 and $1.03 \mu\text{C cm}^{-2}$, respectively, see later) merits further investigation, but electric hysteresis is clear for both materials. These data are typical for H-bonding ferroelectrics.^{5,6} Figure S5 shows the ϵ' vs *T* and P vs *E* measurements with $E//a$ axis for **1Mn**, **2Fe**, **3Co**, and **5Zn**. The dielectric constants of the four compounds along the *a* axis are obviously weaker than those along the *c* axis, and there are no dielectric anomaly peaks in the temperature range investigated. Below the phase transition temperatures, only weak responses and no hysteresis loops were observed in the P vs *E* traces (Figure S5, inset). These results reveal the high anisotropy of the polarization within the materials, and the preferred polarization direction is the *c* direction.

The structures of **1Mn**, **2Fe**, and **3Co** at both 290 and 110 K were determined or re-determined, and the previously reported

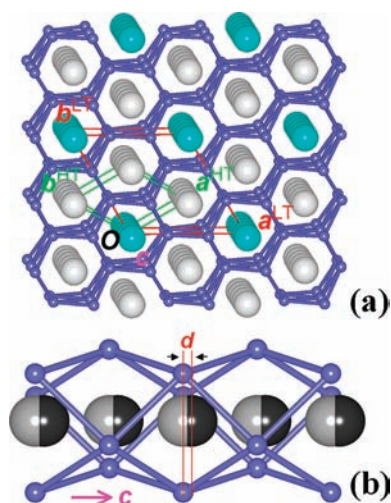


Figure 4. (a) Structure of **1Mn** as a representative, viewed along the c direction. The anionic framework is topologically presented, in which violet-blue spheres are Mn^{2+} and sticks HCOO^- . Green and red boxes are unit cells at 290 and 110 K, respectively. Large spheres are N atoms of NH_4^+ , cyan in the channels at $(0,0,z)$, shifting positively along the c direction (forward), and white in channels at $(\frac{2}{3}, \frac{1}{3}, z)$ and $(\frac{1}{3}, \frac{2}{3}, z)$, shifting negatively along the c direction (backward). (b) Side view of the channel at $(0,0,z)$. Large, light gray spheres are N atoms of NH_4^+ (at HT) showing zero shift with respect to the anionic framework, and large, black spheres are N atoms of NH_4^+ (at LT) showing the shift in d with respect to the anionic framework along the $+c$ direction (toward right).

structures of **4Ni**^{15a} (293 K) and **5Zn**¹⁴ (290 and 110 K) are incorporated (Figure 4, Tables S1–S4). The compounds are isostructural at both low and high temperatures (here after LT and HT), despite the still unavailable LT structure of **4Ni**, and undergo the same structural changes during the phase transition as described previously for **5Zn**.¹⁴ Briefly, the structural changes are as follows: First, the triplet of the unit cell occurs, in which c^{LT} is slightly longer than c^{HT} , $a^{\text{LT}} = (a - b)^{\text{HT}}$, and $V^{\text{LT}} = 3V^{\text{HT}}$ (Figure 4a). Therefore, the unique channel at $(0,0,z)$ in the HT structure becomes three unique channels at $(0,0,z)$, $(\frac{2}{3}, \frac{1}{3}, z)$, and $(\frac{1}{3}, \frac{2}{3}, z)$ in the LT phase, each accommodating one array of ordered NH_4^+ cations. Second, the space group alternates from $P6_322$ (HT) to the polar $P6_3$ (LT) (Table S1), indicating the broken symmetry for the occurrence of ferroelectricity. Third, the disordered NH_4^+ of the trigonal antiprism changes to ordered tetrahedral NH_4^+ , with the change from six apparent but four real N–H···O H-bonds to three real strong N–H···O H-bonds, each for one basal N–H, and a trifurcate acceptor-type N–H···O₃ H-bond for the apical N–H group, with the N–H directing along the c axis (Table S3). Finally and most importantly, in the unit cell of the LT structures (Figure 4a), the NH_4^+ cations in channels at $(0,0,z)$, $(\frac{2}{3}, \frac{1}{3}, z)$, and $(\frac{1}{3}, \frac{2}{3}, z)$ shift d_{N1} , d_{N2} , and d_{N3} , with the d values in the range of 0.359(7)–0.482(4) Å (Table S3), along the c direction, with respect to the anionic framework, compared to the zero d in HT structures (Figure 4b). These shifts or displacements in LT phases directly result in the polarization or the ferroelectricity of the materials. In fact, as the six dipoles were produced in the three channels (two per channel) within the unit cell, four in the same direction ($-c$) and two opposite ($+c$), the dipoles could not be compensated (Figure 4a), and polarization occurred. The P_s values thus could be estimated to be 0.94–1.03 $\mu\text{C cm}^{-2}$ (Table S3)

for **1Mn**, **2Fe**, **3Co**, and **5Zn** from the d data in the available LT structures (at 110 K). The high anisotropy of the polarization (along the c direction) can also be easily elucidated by this mechanism.

Along the series, the members show a systematic decrease in lattice dimensions and interatomic distances of M–O and M···M from **1Mn** to **4Ni**, with **5Zn** close to **3Co** (Tables S1–S3), in good agreement with the change in ionic radii of the divalent metal ions, indicating the shrinkage of the metal–formate frameworks, as observed in other series.^{9,13b} The framework space volume for accommodating one NH_4^+ cation, calculated by PLATON,²⁰ is 28.8–32.2 Å³ at room temperature, but 20.1–21.1 Å³ (averaged) at 110 K. Considering that the vdW volume²¹ of NH_4^+ is 24.3 Å³, these data suggest that the metal–formate framework shrinkage upon cooling results in the shift of NH_4^+ cations with respect to the anionic framework, as well as the double potential wells for NH_4^+ cation in the channel. At 290/293 K, N atoms of NH_4^+ in all structures have quite elongated thermal ellipsoids with their long axes along the c direction, but at 110 K, all N atoms show normal thermal ellipsoids (Table S4). This clearly revealed that, within the channel, the potential well for NH_4^+ movement changes from a quite flat single well at HT to a double well at LT. The movement or disorder of NH_4^+ cations should contribute to the relaxor-like behavior or relaxation.^{18,19} Another interesting and important observation is that the phase transition temperature decreases for smaller metal ions within the series. While the framework shrinks along the a and b directions, it expands along the c axis upon cooling. If we consider the disorder–order transition of NH_4^+ cations in the channel as a 1D liquid–solid transition with the confinement of the framework, the expanding c axis indicates volume expansion during the liquid–solid transition, analogous to the water–ice transition. Therefore, when the radius of the metal ion decreases, the framework becomes smaller, which means higher (internal) pressure for the 1D liquid–solid transition, together with lower freezing temperatures, as observed for the well-known water–ice transition under pressure. Many ferroelectrics, such as BaTiO_3 and KDP, show pressure-induced decreases in their critical temperatures.⁵ The $[(\text{CH}_3)_2\text{NH}_2]\text{[M(HCOO)}_3]$ series also shows a similar dependence of the phase transition temperature on the metal ion.¹¹ We have observed that the mixed-metal series of $[\text{NH}_4][\text{Mn}_{1-x}\text{Zn}_x(\text{HCOO})_3]$ showed a systematic decrease of the phase transition temperature with the increasing Zn component,²² and these results will be reported in the future.

In conclusion, this work demonstrates that magnetic and electric orderings coexist in the magnetic members of the family of $[\text{NH}_4][\text{M(HCOO)}_3]$, and this could be expected for a new class of MOF-based multiferroics. These materials display a paraelectric-to-ferroelectric phase transition between 191 and 254 K, triggered by a disorder–order transition of NH_4^+ cations and their displacement within the confined spaces of metal–formate frameworks. They are highly anisotropic, with the c axis as the polarization axis. The transition temperatures depend upon the metal ions, being lower for smaller ones. The magnetic members within the series show weak ferromagnetism in the low-temperature region. Further research could focus on, for example, (a) variable-temperature X-ray or neutron diffraction and thermodynamic studies to reveal the characteristics and details of the phase transition procedure; (b) investigation of the Ni member when a large crystal becomes available, the mixed-metal systems, and the dielectric relaxation of the Mn and Fe members and its origin; and (c) possible magnetoelectric effects. This research is in progress.

■ ASSOCIATED CONTENT

S Supporting Information. Experimental details, Tables S1–S4, Figures S1–S5, and CIF file. This material is available free of charge via the Internet at <http://pubs.acs.org>.

■ AUTHOR INFORMATION

Corresponding Author

zmw@pku.edu.cn; xiongrg@seu.edu.cn; gaosong@pku.edu.cn

■ ACKNOWLEDGMENT

This work was supported by the NSFC (Grants 20871007, 20821091), the National Basic Research Program of China (Grant 2006CB601102, 2009CB929403), and the China Postdoctoral Science Foundation (Grant 20090450232).

■ REFERENCES

- (1) (a) Cheetham, A. K.; Rao, C. N. R. *Science* **2007**, *318*, 58. (b) Rao, C. N. R.; Cheetham, A. K.; Thirumurugan, A. *J. Phys.: Condens. Matter* **2008**, *20*, 083202.
- (2) For example: (a) Long, J. R.; Yaghi, O. M., Eds. Special issue on metal–organic frameworks. *Chem. Soc. Rev.* **2009**, *38*, 1213. (b) Janiak, C.; Vieth, J. K. *New J. Chem.* **2010**, *34*, 2366.
- (3) (a) Miller, J. S.; Gatteschi, D., Eds. Thematic issue on molecule-based magnets. *Chem. Soc. Rev.* **2011**, *40*, 3065. (b) Coronado, E.; Dunbar, K. R., Eds. Special issue for the Forum on Molecular Magnetism: The Role of Inorganic Chemistry. *Inorg. Chem.* **2009**, *48*, 3293.
- (4) (a) Hang, T.; Zhang, W.; Ye, H.-Y.; Xiong, R.-G. *Chem. Soc. Rev.* **2011**, *40*, 3577. (b) Guo, M.; Cai, H.-L.; Xiong, R.-G. *Inorg. Chem. Commun.* **2010**, *13*, 1590. (c) Zhou, B.; Kobayashi, A.; Cui, H.-B.; Long, L.-S.; Fujimori, H.; Kobayashi, H. *J. Am. Chem. Soc.* **2011**, *133*, 5736. (d) Zhao, H.-X.; Kong, X.-J.; Li, H.; Jin, Y.-C.; Long, L.-S.; Zeng, X.-C.; Huang, R.-B.; Zheng, L.-S. *Proc. Natl. Acad. Sci. U.S.A.* **2011**, *108*, 3481.
- (5) (a) Lines, M. E.; Glass, A. M. *Principles and Applications of Ferroelectrics and Related Materials*; Clarendon Press: Oxford, 1977. (b) Jona, F.; Shirane, G. *Ferroelectric Crystals*; Pergamon Press: Oxford, 1962.
- (6) (a) Horiuchi, S.; Tokunaga, Y.; Giovannetti, G.; Picozzi, S.; Itoh, H.; Shimano, R.; Kumai, R.; Tokura, Y. *Nature* **2010**, *463*, 789. (b) Horiuchi, S.; Tokura, Y. *Nat. Mater.* **2008**, *7*, 357.
- (7) Ramesh, R. *Nature* **2009**, *461*, 1218.
- (8) (a) Kimura, T.; Goto, T.; Shintani, H.; Ishizaka, K.; Arima, T.; Tokura, Y. *Nature* **2003**, *426*, 55. (b) Cheong, S.-W.; Mostovoy, M. *Nat. Mater.* **2007**, *6*, 13. (c) Wang, K. F.; Liu, J. -M.; Ren, Z. F. *Adv. Phys.* **2009**, *58*, 321. (d) Scott, J. F.; Blinc, R. J. *J. Phys.: Condens. Matter* **2011**, *23*, 113202.
- (9) Wang, Z. M.; Hu, K. L.; Gao, S.; Kobayashi, H. *Adv. Matter* **2010**, *22*, 1526 and references cited therein.
- (10) (a) Cui, H. B.; Takahashi, K.; Okano, Y.; Kobayashi, H.; Wang, Z. M.; Kobayashi, A. *Angew. Chem., Int. Ed.* **2005**, *44*, 6508. (b) Cui, H. B.; Wang, Z. M.; Takahashi, K.; Okano, Y.; Kobayashi, H.; Kobayashi, A. *J. Am. Chem. Soc.* **2006**, *128*, 15074.
- (11) (a) Jain, P.; Ramachandran, V.; Clark, R. J.; Zhou, H. D.; Toby, B. H.; Dalal, N. S.; Kroto, H. W.; Cheetham, A. K. *J. Am. Chem. Soc.* **2009**, *131*, 13625. (b) Jain, P.; Dalal, N. S.; Toby, B. H.; Kroto, H. W.; Cheetham, A. K. *J. Am. Chem. Soc.* **2008**, *130*, 10450. (c) Sánchez-Andújar, M.; Presedo, S.; Yáñez-Vilar, S.; Castro-García, S.; Shamir, J.; Señaris-Rodríguez, M. A. *Inorg. Chem.* **2010**, *49*, 1510.
- (12) (a) Wang, Z. M.; Zhang, B.; Otsuka, T.; Inoue, K.; Kobayashi, H.; Kurmoo, M. *Dalton Trans.* **2004**, 2209. (b) Wang, X. Y.; Gan, L.; Zhang, S. W.; Gao, S. *Inorg. Chem.* **2004**, *43*, 4615.
- (13) (a) Stroppa, A.; Jain, P.; Barone, P.; Marsman, M.; Perez-Mato, J. M.; Cheetham, A. K.; Kroto, H. W.; Picozzi, S. *Angew. Chem., Int. Ed.* **2011**, *50*, 5847. (b) Hu, K. L.; Kurmoo, M.; Wang, Z. M.; Gao, S. *Chem.–Eur. J.* **2009**, *15*, 12050.
- (14) Xu, G. C.; Ma, X. M.; Zhang, L.; Wang, Z. M.; Gao, S. *J. Am. Chem. Soc.* **2010**, *132*, 9588.
- (15) (a) Wang, Z. M.; Zhang, B.; Inoue, K.; Fujiwara, H.; Otsuka, T.; Kobayashi, H.; Kurmoo, M. *Inorg. Chem.* **2007**, *46*, 437. (b) Chen, Y. H. B.Sc. Thesis, Peking University, 2008. (c) Xu, G. C.; Ma, X. M.; Zhang, L.; Wang, Z. M.; Gao, S. Presented at the 12th International Conference on Molecule-based Magnetism, Beijing, China, October 2010.
- (16) (a) Samantaray, R.; Clark, R. J.; Choi, E. S.; Zhou, H.; Dalal, N. S. *J. Am. Chem. Soc.* **2011**, *133*, 3792. (b) Szklarz, P.; Chański, M.; Ślepokura, K.; Lis, T. *Chem. Mater.* **2011**, *23*, 1082.
- (17) Carlin, R. L. *Magnetochemistry*; Springer-Verlag: Berlin/Heidelberg, 1986; pp 148–154.
- (18) (a) Samara, G. A. *J. Phys.: Condens. Matter* **2003**, *15*, R367. (b) Bokov, A. A.; Ye, Z.-G. *J. Mater. Sci.* **2006**, *41*, 31. (c) Kleemann, W. *J. Mater. Sci.* **2006**, *41*, 129.
- (19) (a) Szafranski, M.; Katrusiak, A. *J. Phys. Chem. B* **2008**, *112*, 6779. (b) Szafranski, M.; Katrusiak, A.; McIntyre, G. J. *Cryst. Growth Des.* **2010**, *10*, 4334.
- (20) Spek, A. L. *PLATON, A Multipurpose Crystallographic Tool*; Utrecht University: Utrecht, The Netherlands, 2001.
- (21) This was calculated using PCMODEL Version 9.1; see <http://www.serenasoft.com>.
- (22) Ma, X. M. B.Sc. Thesis, Peking University, 2009.